the procedure of Nicholson *et al.* (8). This procedure was carried out for dimethyl fumarate and cinnamonitrile in the region where i_{pa}/i_{pc} is most sensitive to variations in k_2. The i_{pa} values for fumaronitrile were too small to allow precise calculations from cyclic voltammetric data. The results and some intermediate factors used in the calculations are shown in Table III. The k_2 values obtained for dimethyl fumarate and cinnamonitrile are 1.6×10^2 and 7.9×10^2 liters/mole-sec, respectively.

Discussion

The results obtained here support the previous studies (1) and point to the major pathway in the electrohydrodimerization of these compounds as involving initial production of the anion radical followed by a coupling step. Other aspects of the mechanism, the protonation steps, the nature of the polymerization reaction, and the reactions at the later waves, which sometimes lead to secondary radicals (10), still await elucidation.

In examining the results, we see that dimethyl fumarate, which undergoes dimerization at the slowest rate of the three compounds, shows the most scatter in the k_2 value calculated from RRDE results and only fair agreement with that obtained by cyclic voltammetry. Several factors contribute to this. Because the radical ion disappearance is slow on the RRDE time scale, N_K values are close to those for an unperturbed collection efficiency, and the observed slopes are rather insensitive to small changes in *XKTC*. Moreover, the small value of k_2 necessitates use of high dimethyl fumarate concentrations, which increases the polymerization side reaction.

The RRDE results for cinnamonitrile fall into the sensitive N_K *vs. CONI* region for our electrode and the reaction is unperturbed by polymerization. The k_2 values determined by RRDE measurements over a wide range of C and for differing ω show good precision and agree very well with the value determined by cyclic voltammetry. This good agreement between a steady-state and transient technique also is suggestive of lack of involvement of adsorption of parent or intermediates in the reaction mechanism.

The fumaronitrile RRDE experiments were performed near the upper limit of determinable k_2 values with our RRDE. For this reaction, for concentrations of 0.4 to 4 mM, N_K values of only 0.020-0.006 (*CONI* = 1) were found. For both the cinnamonitrile and fumaronitrile reactions the data suggest some contribution from a reaction of the anion radical with parent, although in both cases this contribution was relatively small. It is interesting that even this small contribution can be noticed and accounted for in the analysis of the data, although other processes removing anion radical, such as a first order ECE reaction leading to RH_2, may also account for the small deviations from a close fit to mechanism I.

Acknowledgment

The support of the Robert A. Welch Foundation and the National Science Foundation (GP 6688X) are gratefully acknowledged. We also thank Dr. Ira B. Goldberg for helpful suggestions.

Manuscript submitted Dec. 17, 1971; revised manuscript received March 20, 1972.

Any discussion of this paper will appear in a Discussion Section to be published in the June 1973 JOURNAL.

REFERENCES

1. W. V. Childs, J. T. Maloy, C. P. Keszthelyi, and A. J. Bard, *This Journal*, **118**, 874 (1971).
2. V. J. Puglisi and A. J. Bard, *This Journal*, **119**, 833 (1972).
3. M. Baizer, *This Journal*, **111**, 215 (1964).
4. T. Asahara, M. Seno, and M. Tsuchiya, *Bull. Chem. Soc. Japan*, **42**, 2416 (1969).
5. M. Baizer and J. D. Anderson, *This Journal*, **111**, 223 (1964).
6. J. Petrovich, M. Baizer, and M. Ort, *ibid.*, **116**, 749 (1969).
7. L. R. Faulkner and A. J. Bard, *J. Am. Chem. Soc.*, **90**, 6284 (1968).
8. M. L. Olmstead, R. G. Hamilton, and R. S. Nicholson, *Anal. Chem.*, **41**, 225 (1969).
9. C. P. Andrieux, L. Nadjo, and J. M. Saveant, *J. Electroanal. Chem.*, **26**, 147 (1970).
10. I. Goldberg and A. J. Bard, Unpublished experiments, Univ. of Texas, 1971.

Rotating Ring-Disk Electrodes

IV. Dimerization and Second Order ECE Reactions

Vincent J. Puglisi and Allen J. Bard*

Department of Chemistry, The University of Texas at Austin, Austin, Texas 78712

ABSTRACT

Digital simulation techniques have been employed to compute the steady-state currents at the rotating ring-disk electrode (RRDE) as functions of a rate parameter exhibiting explicit dependence on concentration of parent species (A) and rotation rate and also as functions of the flux at the disk for those cases in which the disk generated product (B) undergoes a following dimerization EC reaction ($2B \rightarrow$ products) or a second order ECE reaction ($B + A \rightarrow C$, where C may be electroactive at the disk potential) and nuances thereof. Diagnostic criteria are given for using RRDE results to distinguish among possible reaction mechanisms and working curves are provided to allow calculation of the rate constants of the homogeneous reactions.

The rotating ring-disk electrode (RRDE) has been used to study electrogenerated intermediates which react by different schemes (1). Past papers in this series (2-4) have discussed the use of digital simulation techniques to treat the currents at the disk and the ring of the RRDE and discussed methods for extracting kinetic information about the reactions of the disk-generated species. In this paper results of the digital simulation of reaction mechanisms in which the disk generated species can couple with itself (dimerization) or with the parent compound are presented. Many examples of actual electrode reactions which proceed by mechanisms such as these can be given; particular current interest centers around reductive coupling reactions of activated olefins or elec-

* Electrochemical Society Active Member.
Key words: digital simulation, hydrodimerization reactions, rotating disk electrode, electrode reactions.

trohydrodimerizations [see (5-6) and references contained therein].

The following mechanisms are considered:

I. Dimerization EC (electrochemical-chemical) — Species B, which is generated at the disk electrode by

$$A + n_1e \rightarrow B \qquad [1]$$

dimerizes to a nonelectroactive product

$$2B \xrightarrow{k_2} X \qquad [2]$$

At the ring electrode A is regenerated from B by the reaction

$$B - n_1e \rightarrow A \qquad [3]$$

II. Second order ECE.—Species B, produced at the disk as in Eq. [1], reacts with parent

$$B + A \xrightarrow{k_2} C \qquad [4]$$

where C is immediately reduced at the disk

$$C + n_2e \rightarrow Z \qquad [5]$$

At the ring electrode either (*a*) B alone is oxidized, as in Eq. [3], or (*b*) both B and C are oxidized. Nuances of ECE mechanism IIa (7-8) consider (*c*) the irreversible reaction represented in Eq. [4] or (*d*) the reversible reaction

$$B + A \rightleftarrows C \quad K_{Eq.} \qquad [6]$$

followed by an irreversible oxidation-reduction charge transfer reaction

$$B + C \xrightarrow{k_2'} Z + A \qquad [7]$$

III. Second order EC.—Species B, produced at the disk as in Eq. [1], reacts with parent to form a nonelectroactive product

$$B + A \xrightarrow{k_2} Y \qquad [8]$$

Again at the ring B oxidizes to A via Eq. [3].

Note that these three mechanisms represent possible paths from A to a coupled product (X, Y, or Z). The treatment below is aimed at computing how the collection efficiency, N_K,

$$N_K = |i_r/i_d| \qquad [9]$$

where i_r and i_d are the ring and disk currents, respectively, varies with concentration of parent, C, rotation rate, ω, i_d, and the rate constants of the reactions consuming B and at establishing criteria for distinguishing between these mechanisms. The application of the RRDE to the elucidation of the mechanism of electrohydrodimerization of dimethyl fumarate, cinnamonitrile, and fumaronitrile is demonstrated in the accompanying paper (9).

Digital Simulation

The general approach to the simulations and the notation to be used has been described in the previous communications (2-4). Two different types of experiments were simulated. In the first the disk was assumed to be held at a potential where the concentration of A at the disk surface was always zero and for mechanism II, the concentration of C at the disk surface was also zero. A second simulation concerned a constant current maintained at the disk, so that the flux of A (or the sum of the fluxes of A and C in mechanism II) was held constant at the disk. In both cases the boundary condition at the ring electrode was that the concentration of B was zero at the ring. In mechanism IIb, the concentration of C was also held at zero at the ring surface. Surface boundary conditions for the different experiments and mechanisms considered are given in Table I. As in previous simulations, the results are specific for the particular RRDE geometry considered. The electrode under consideration here had IR1 = 94, IR2 = 100, and IR3 = 166, where IR1, IR2, and IR3 are the number of simulation boxes necessary to represent the radius of the disk electrode, and the radii to the inner and outer edge of the ring electrode, respectively; these values yield a collection efficiency in the absence of kinetic perturbations of 0.555. Values of i_d, i_r, and N_K were calculated as functions of the dimensionless parameter $XKTC$ in the controlled

$$XKTC = (0.51)^{-2/3}\nu^{1/3}D^{-1/3}C_A^{\circ}\omega^{-1}k_2 \qquad [10]$$

potential simulation and as functions of $XKTC$ and the flux at the disk in the constant disk current simulation. Because a basic assumption of mechanism II is that species C is more easily reduced than species A, it was first necessary to establish in the constant current simulation if the total flux at the disk, as defined by the current, was greater or less than the maximum flux possible for species C. If greater, a fraction of the total current was allocated sufficient to maximize the concentration gradient of C at the disk surface

Table I. Surface boundary conditions

	Boundary conditions ($x = 0$)		
	$t < 0$	$t \geq 0$	
Mechanism	Disk and ring	Disk	Ring
	A. Controlled disk potential		
I	$C_A = C_A^{\circ}$ $C_B = 0$	$C_A = 0$ $C_B = C_A^{\circ}$	$C_A = C_A'$ $C_B = 0$
IIa	$C_A = C_A^{\circ}$ $C_B = 0$ $C_C = 0$	$C_A = 0$ $C_B = C_A^{\circ}$ $C_C = 0$	$C_A = C_A'$ $C_B = 0$ $C_C = C_C'$
IIb	$C_A = C_A^{\circ}$ $C_B = 0$ $C_C = 0$	$C_A = 0$ $C_B = C_A^{\circ}$ $C_C = 0$	$C_A = C_A'$ $C_B = 0$ $C_C = 0$
IIc	$C_A = C_A^{\circ}$ $C_B = 0$ $C_C = 0$	$C_A = 0$ $C_B = C_A^{\circ}$ $C_C = 0$	$C_A = C_A'$ $C_B = 0$ $C_C = C_C'$
IId	$C_A = C_A^{\circ}$ $C_B = 0$ $C_C = 0$	$C_A = 0$ $C_B = C_A^{\circ}$ $C_C = 0$	$C_A = C_A'$ $C_B = 0$ $C_C = C_C'$
III	$C_A = C_A^{\circ}$ $C_B = 0$	$C_A = 0$ $C_B = C_A^{\circ}$	$C_A = C_A'$ $C_B = 0$
	B. Controlled disk current		
I	$C_A = C_A^{\circ}$	$D_A\left(\frac{\partial C_A}{\partial x}\right)_{x=0} = \frac{i}{nFA}$	$C_A = C_A'$
	$C_B = 0$	$-D_B\left(\frac{\partial C_B}{\partial x}\right)_{x=0} = \frac{i}{nFA}$	$C_B = 0$
IIa	$C_A = C_A^{\circ}$	$D_A\left(\frac{\partial C_A}{\partial x}\right)_{x=0} +$	$C_A = C_A'$
	$C_B = 0$	$D_C\left(\frac{\partial C_C}{\partial x}\right)_{x=0} = \frac{i}{nFA}$	$C_B = 0$
	$C_C = 0$	$-D_B\left(\frac{\partial C_B}{\partial x}\right)_{x=0} = \frac{i}{nFA}$	$C_C = C_C'$
IIb	$C_A = C_A^{\circ}$	$D_A\left(\frac{\partial C_A}{\partial x}\right)_{x=0} +$	$C_A = C_A'$
	$C_B = 0$	$D_C\left(\frac{\partial C_C}{\partial x}\right)_{x=0} = \frac{i}{nFA}$	$C_B = 0$
	$C_C = 0$	$-D_B\left(\frac{\partial C_B}{\partial x}\right)_{x=0} = \frac{i}{nFA}$	$C_C = 0$
IIc	$C_A = C_A^{\circ}$	$D_A\left(\frac{\partial C_A}{\partial x}\right)_{x=0} +$	$C_A = C_A'$
	$C_B = 0$	$D_C\left(\frac{\partial C_C}{\partial x}\right)_{x=0} = \frac{i}{nFA}$	$C_B = 0$
	$C_C = 0$	$-D_B\left(\frac{\partial C_B}{\partial x}\right)_{x=0} = \frac{i}{nFA}$	$C_C = C_C'$
IId	$C_A = C_A^{\circ}$	$D_A\left(\frac{\partial C_A}{\partial x}\right)_{x=0} +$	$C_A = C_A'$
	$C_B = 0$	$D_C\left(\frac{\partial C_C}{\partial x}\right)_{x=0} = \frac{i}{nFA}$	$C_B = 0$
	$C_C = 0$	$-D_B\left(\frac{\partial C_B}{\partial x}\right)_{x=0} = \frac{i}{nFA}$	$C_C = C_C'$
III	$C_A = C_A^{\circ}$	$D_A\left(\frac{\partial C_A}{\partial x}\right)_{x=0} = \frac{i}{nFA}$	$C_A = C_A'$
	$C_B = 0$	$-D_B\left(\frac{\partial C_B}{\partial x}\right)_{x=0} = \frac{i}{nFA}$	$C_B = 0$

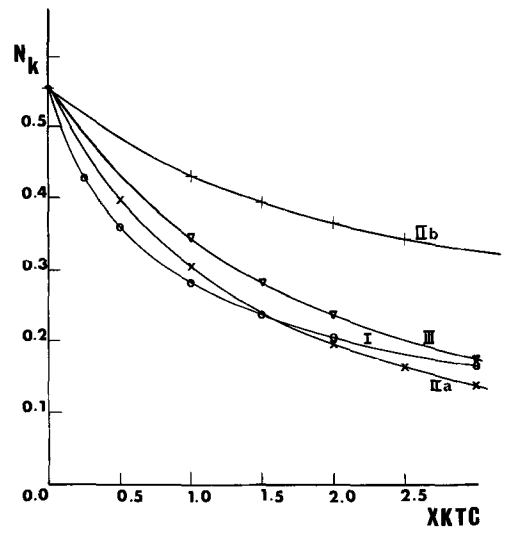

Fig. 1. Collection efficiency (N_K) *vs. XKTC* for the EC dimerization mechanism (I), the ECE radical-parent coupling mechanisms (IIa and IIb), and the EC radical-parent coupling mechanism (III).

[FC(1,1) = 0] while the remaining current diminished the concentration of A. If less, a finite concentration of C remained at the surface and the concentration of A was not altered by the passage of current. In every instance the diffusion coefficients of species A, B, and C were assumed equal, although provision is included in the program for introducing a different value for each species.

Results

Controlled disk potential results.—The results of simulations where the disk potential is maintained on the limiting current plateau for reaction [1] and the ring maintained at a potential where [3] occurs at the mass transfer controlled rate are shown in Fig. 1. [Mechanisms IIc and IId are not shown in Fig. 1 because of N_K's dependence on two parameters (equilibrium constant and rate constant) instead of one for the mechanisms as shown but qualitatively they would show the same sort of behavior.] All curves yield a value of $N_K = N = 0.555$ as *XKTC* approaches 0 (k_2C approaches 0, or ω approaches infinity) and all show a similar decrease of N_K with increasing *XKTC*. While these N_K-*XKTC* curves are indicative of kinetic perturbations and could be used to determine k_2 values once the mechanism is known, they are clearly not very useful in distinguishing among the various mechanisms under consideration. Further, the dependence of the disk limiting current on *XKTC* (Table II) is of value only in distinguishing case III from cases I and II. Case II, categorized as an ECE type, is unlike the simple ECE case in that n, the number of electrons per molecule of starting material, A, electrolyzed, equals one independent of the rotation rate. Case III, however, undergoes a change in n from $n = 1$ to $n = 2$ with increasing rotation rate and thus, exhibits a dependence of disk limiting current with varying *XKTC* values.

Controlled disk current results.—Experiments involving disk currents at values below the limiting one are more diagnostic in deciding among the various reaction schemes under consideration here, because the relative fluxes of A and B from the disk can be varied. Simulations in this case are of N_K at different values of the relative disk current, *CONI*, where

$$CONI = i_d/i_{d,1} \qquad [11]$$

and $i_{d,1}$ is the limiting disk current, and for different values of *XKTC*. In this case a separate N_K *vs. CONI* curve must be given for each value of *XKTC*. Results for the mechanisms under consideration here are given in Fig. 2-7. Note that for a first order decomposition

Table II. Dependence of disk limiting current on *XKTC*

Mechanism	*XKTC*	N_K	ZR[a]	ZD[b]
I	0.5	0.360	0.279	0.776
	1.0	0.281	0.218	0.776
	1.5	0.235	0.183	0.776
	2.0	0.205	0.159	0.776
	3.0	0.165	0.128	0.776
IIa	0.0	0.556	0.432	0.776
	1.0	0.305	0.236	0.776
	2.0	0.194	0.151	0.776
	3.0	0.135	0.105	0.776
IIb	1.0	0.430	0.333	0.776
	2.0	0.366	0.284	0.776
	3.0	0.326	0.253	0.776
	4.0	0.298	0.231	0.776
	6.0	0.260	0.202	0.776
	8.0	0.234	0.182	0.776
III	1.0	0.344	0.236	0.688
	2.0	0.235	0.151	0.643
	3.0	0.170	0.104	0.615
	4.0	0.128	0.076	0.596
	5.0	0.100	0.058	0.581
	8.0	0.052	0.029	0.551

[a] $ZR = \dfrac{i_r}{(0.51)^{1/3} n F A_d C_A^\circ D_B^{2/3} \omega^{1/2} \nu^{-1/6}}$.

[b] $ZD = \dfrac{i_d}{(0.51)^{1/3} n F A_d C_A^\circ D_A^{2/3} \omega^{1/2} \nu^{-1/6}}$.

of B, N_K is independent of *CONI*, at a given value of *XKT*, because both the velocity of the following reaction and the amount of B reaching the ring are proportional to disk current. The trend of N_K with *CONI* is

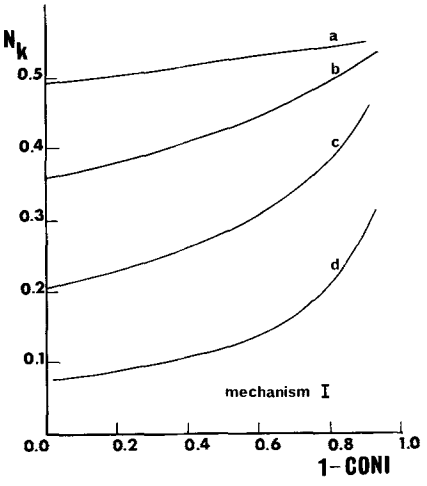

Fig. 2. Collection efficiency (N_K) *vs.* 1-*CONI* for mechanism I and *XKTC* equal to (a) 0.1, (b) 0.5, (c) 2.0, and (d) 10.0, where $CONI = i_d/i_{d,1}$ and $XKTC = (0.51)^{-2/3}\nu^{1/3}D^{-1/3}\omega^{-1}k_2C$.

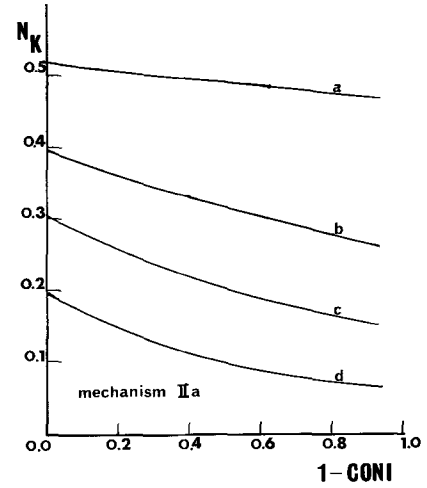

Fig. 3. Collection efficiency (N_K) *vs.* 1-*CONI* for mechanism IIa and *XKTC* equal to (a) 0.1, (b) 0.5, (c) 1.0, and (d) 2.0.

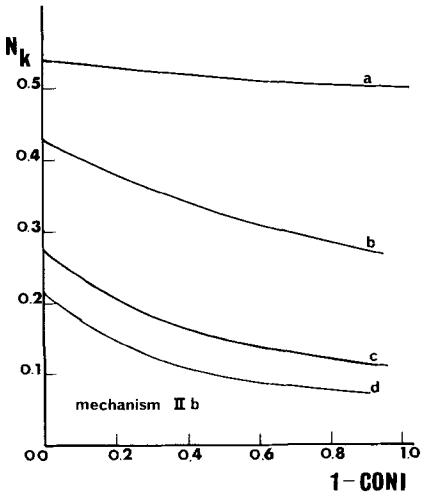

Fig. 4. Collection efficiency (N_K) *vs.* 1-*CONI* for mechanism IIb and *XKTC* equal to (a) 0.1, (b) 1.0, (c) 5.0, and (d) 10.0.

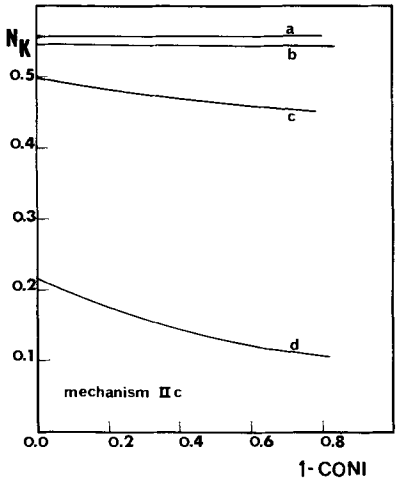

Fig. 5. Collection efficiency (N_K) *vs.* 1-*CONI* for mechanism IIc, *XKTC2* equal to 1000 and *XKTC1* equal to (a) 0.001, (b) 0.010, (c) 0.10, and (d) 1.0, where *XKTC1* and *XKTC2* describe the reactions represented in Eq. [4] and [7], respectively.

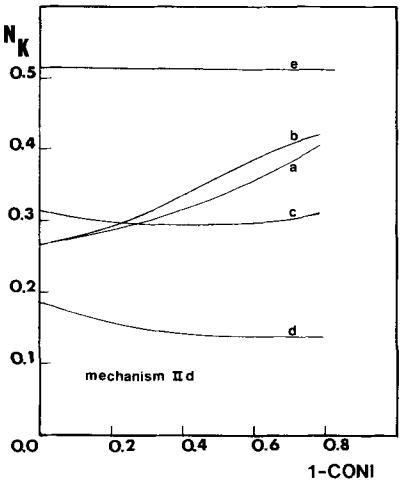

Fig. 6. Collection efficiency (N_K) *vs.* 1-*CONI* for mechanism IId and (a) $CK = 10^{-4}$, $XKTC = 10^5$; (b) $CK = 10^{-3}$, $XKTC = 10^4$; (c) $CK = 10^{-2}$, $XKTC = 10^3$; (d) $CK = 10^{-1}$, $XKTC = 10^2$, and (e) $CK = 10^{-3}$, $XKTC = 10^3$.

qualitatively different for cases I and IIa (or IIb, IIc, III). For mechanism I, the dimerization EC reaction, the velocity of the following reaction only depends on B concentration. Hence, as i_d becomes smaller (*CONI* approaches 0), the B concentration at the disk decreases and the kinetic perturbation of the following reaction becomes less. Hence, for case I, $N_K \rightarrow N$ as $CONI \rightarrow 0$ and N_K approaches its minimum value as $CONI \rightarrow 1$. For cases IIa, IIb, IIc, or III, which involve coupling with the parent, the rate of the following reaction is a function of both A and B concentration at the disk. Hence, as i_d approaches $i_{d,1}$ (*CONI* approaches 1) the A concentration decreases and the following reaction rate decreases. For these cases N_K approaches its maximum value at a given value of *XKTC* as $CONI \rightarrow 1$. As *CONI* approaches 0, the concentration of A is essentially constant and the reaction of B approaches pseudo-first order conditions. When product C is also electroactive at the ring electrode (mechanism IIb), the trend is the same as for mechanism IIa but the N_K values are larger because i_r is larger. Although case IId exhibits qualitatively different behavior depending on the value of the equilibrium constant for [6] and the rate constant for [7] as shown in Fig. 6, some trends are evident. For values of *CK* (*CK* = bulk concentration of A × equilibrium constant (*K*) for reaction [6]) greater than or equal to 0.10 and *XKTC* values resulting in collection efficiencies in the normal working range for the simulated RRDE ($0.02 < N_K < 0.54$), N_K approaches its maximum value as $CONI \rightarrow 1$. As $CONI \rightarrow 0$, the concentration of C is essentially constant and the reaction consuming B approaches pseudo-first order behavior. For *CK* values less than or equal to 0.001 (*e.g.*, $K = 1$ when $C = 1$ mM), the N_K variation with *CONI* is qualitatively similar to case I because the velocity of the following reaction assumes an over-all second order dependence on B concentration. Transitional behavior, exemplified by curves b, c, and e (Fig. 6), occurs at intermediate values of *CK*. Quantitatively, the behavior of case IId differs from that of case I, for all values of *CK*, because the product of the appropriate dimensionless simulation parameters for case IId (*i.e.*, *CK* and *XKTC*), which defines the velocity of the reactions consuming species B (and thus the magnitude of N_K) has a squared dependence on the bulk concentration of A, whereas for case I, the reaction velocity is described by only one dimensionless simulation rate parameter, *XKTC*.

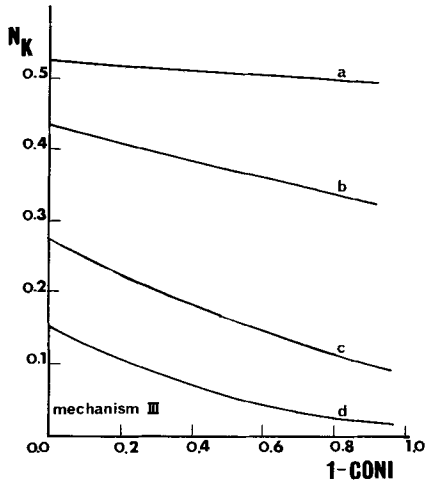

Fig. 7. Collection efficiency (N_K) *vs.* 1-*CONI* for mechanism III and *XKTC* equal to (a) 0.1, (b) 0.5, (c) 2.0, and (d) 5.0.

Discussion

The results show that the RRDE should be useful in studying different mechanisms of following reactions. Since RRDE studies involving steady-state N_K measurements are relatively free from adsorption and double layer charging effects, the experimental results will be subject to fewer complications than transient methods. Digital simulation methods are capable of treating rather complex reaction schemes involving higher order chemical reactions. Variations of the mechanisms considered here, such as the simultaneous

occurrence of two of the reaction paths, can be treated by straightforward extensions of the described programs. For example, in studies of hydrodimerization reactions with the RRDE (9) it was sometimes necessary to consider the possibility of parallel reaction pathways of the intermediate radical ion (equivalent to substance B here) by both coupling and ECE mechanisms. The results in that work provide experimental confirmation of these theoretical results.

Acknowledgment

The support of the Robert A. Welch Foundation and the National Science Foundation (GP6688X) are gratefully acknowledged.

Manuscript submitted Dec. 17, 1971; revised manuscript received March 20, 1972.

Any discussion of this paper will appear in a Discussion Section to be published in the June 1973 JOURNAL.

REFERENCES

1. W. J. Albery and M. L. Hitchman, "Ring-Disc Electrodes," Oxford University Press, London (1971).
2. K. B. Prater and A. J. Bard, *This Journal*, **117**, 207 (1970).
3. *Ibid.*, 335 (1970).
4. *Ibid.*, 1517 (1970).
5. W. C. Childs, J. T. Maloy, C. P. Keszthelyi, and A. J. Bard, *ibid.*, **118**, 874 (1971).
6. M. M. Baizer, J. P. Petrovich, and D. A. Tyssee, *ibid.*, **117**, 173 (1970).
7. M. D. Hawley and S. W. Feldberg, *J. Phys. Chem.*, **70**, 3459 (1966).
8. L. Nadjo and J. M. Saveant, *J. Electroanal. Chem.*, **33**, 419 (1971).
9. V. J. Puglisi and A. J. Bard, *This Journal*, **119**, 829 (1972).

Electrochemical Reduction of Allopurinol

P. K. De and Glenn Dryhurst

Department of Chemistry, University of Oklahoma, Norman, Oklahoma 73069

ABSTRACT

Allopurinol (1H-pyrazolo [3,4-d] pyrimidin-4-ol) is electrochemically reduced at the dropping mercury electrode by way of a single polarographic wave. Above pH 2, the electrode reaction is a $2e$-$2H^+$ reduction of allopurinol to give 6,7-dihydroallopurinol as the sole product. At lower pH (*i.e.*, pH 0) the single polarographic wave involves $4e$ and is due to reduction of allopurinol to 2,3,6,7-tetrahydroallopurinol. Under the conditions of prolonged electrolysis, however, the latter product slowly decomposes to give 4-carbamido-5 aminopyrazoline (2,3). The mechanism of these reactions have been elucidated by polarography, coulometry, cyclic voltammetry at the pyrolytic graphite electrode, mass electrolysis and isolation of products. The products have been identified by u.v., *IR*, NMR, mass spectrometry, and elemental analysis.

Pyrazolo [3,4-d] pyrimidines have found considerable application in clinical biochemistry as carcinostatic agents. Allopurinol (1H-pyrazolo [3,4-d] pyrimidine 4-ol) is a well-known inhibitor of the enzyme xanthine oxidase (1), and, hence, inhibits the formation of uric acid by oxidation of purines in organisms containing this enzyme (2, 3). This property of allopurinol makes it possible to use lower doses of otherwise highly toxic 6-thiopurine in the treatment of leukemia (4). Allopurinol also substantially alters pyrimidine metabolism (5).

Because of the importance of understanding the oxidation-reduction behavior of biologically important compounds which interact with oxidation-reduction enzymes, we have begun a detailed and systematic study of the electrochemistry of the allopurines. The structure of allopurinol and the numbering employed in this paper is that used in "Chemical Astracts," and is shown below.

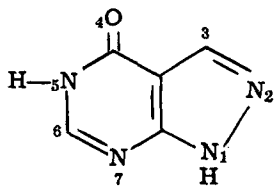

Experimental

Chemicals.—Allopurinol was obtained from Aldrich and was found to be chromatographically homogeneous. The other chemicals were of reagent grade. Argon (Linde) used for deoxygenating was equilibrated with water; no other purification was necessary. Buffer solutions used had an ionic strength of 0.5*M* except sulfuric and acetic acid solutions which were 1*M* in strength.

Key words: 1H-pyrazolo [3,4-d] pyrimidin-4-ol, bioelectrochemistry, 6,7-dihydroallopurinol, 2,3,6,7-tetrahydroallopurinol.

Apparatus.—The electrochemical apparatus has been described elsewhere (6-8). All potentials are referred to the SCE at 25°C. The dropping mercury electrode had normal m and t values.

Ultraviolet absorption spectra were recorded on a Perkin Elmer-Hitachi Model 124 spectrophotometer. Infrared spectra were recorded on a Beckman *IR*-8 using KBr pellets. NMR spectra were recorded on Varian Model T-60 spectrometer. Mass spectra were recorded on a Hitachi Model RMU-6E spectrometer.

Coulometry and macroscale electrolysis.—For coulometry a measured volume (usually 100 ml) of background solution was introduced into the working electrode compartment of a three compartment cell. This solution was electrolyzed at the appropriate potential until an electronic current integrator gave a constant and small count. Then a weighed amount of allopurinol was introduced into the working electrode compartment sufficient to make the solution *ca.* 1 mM. After dissolution electrolysis was recommenced at the same potential, stirring rate, and flow rate of argon. Many macroscale electrolyses were carried out in the same fashion except that solutions were *ca.* 5-6 mM in allopurinol and an integrator was not employed. Completion of the electrolysis was confirmed by disappearance of the characteristic u.v. absorption and polarographic wave of allopurinol, and by characteristic cyclic voltammetric behavior at the pyrolytic graphite electrode.